Bull. Mater. Sci., Vol. 37, No. 5, August 2014, pp. 1137–1146. © Indian Academy of Sciences.

Effect of ethyl vanillin on ZnNi alloy electrodeposition and its properties

K O NAYANA and T V VENKATESHA*

Department of Chemistry, School of Chemical Sciences, Kuvempu University, Shankaraghatta 577 451, India

MS received 16 July 2013; revised 30 October 2013

Abstract. The bright ZnNi alloy coating on steel surface was prepared by elctrodepostion technique using brightener ethyl vanillin (EV). To know the influence of brightener on deposition and dissolution behaviour of ZnNi alloy, cyclic voltammetric studies were carried out. FT–IR spectroscopic evidence was given to confirm selective adsorption of brightener on steel surface. The brightener enhances current efficiency and throwing power of plating bath during coating. The scanning electron microscopy (SEM) and X-ray diffraction (XRD) analyses in presence of brightener confirmed the change in surface morphology, phase composition and preferred orientation of ZnNi coating. In presence of brightener, nickel content of the coating was reduced at higher current density and thickness. In addition, deposit properties like appearances, hardness, adherence, ductility and corrosion resistance of ZnNi alloy deposits were also improved in bright deposit. Simultaneously, effect of deposition current density and thickness on corrosion behaviour of coating was examined.

Keywords. Corrosion resistance; microhardness; X-ray diffraction; ZnNi alloy; electrodeposition; ethyl vanillin.

1. Introduction

Among the various coating techniques, zinc electrodepostion was widely used to protect steel from corrosion. But, zinc coating undergo rapid corrosion in aggressive environment (Pushpavanam 2000; Kim *et al* 2003). Alternatively, alloying of zinc with iron group metal such as Ni, Fe and Co enhances anti-corrosion property of conventional zinc coating (Kautek *et al* 1994; Pech-Canul *et al* 1997). Among the various zinc alloys, ZnNi showed the best corrosion resistance and mechanical properties like microhardness, wear resistance, ductility, strength, adheres, etc. In addition, ZnNi alloy also serves as substitute for toxic cadmium coating. These coatings substantially provide better sacrificial protection at 10−12% of Ni (Pushpavanam *et al* 1991; Brooks and Erb 2001; Bajat *et al* 2005).

ZnNi alloy coatings were deposited from alkaline and acid baths. Acid bath was used more often, owing to its high deposition rate and cathodic efficiency. Moreover, this bath does not require complexing agents, leading to less expensive deposition process than alkaline plating bath (Li *et al* 2007). Organic additives were often added to alloy plating bath, which improves the properties of deposits. It make the surface more durable, uniform and compact for better performance in terms of corrosion protection and mechanical properties (Sachin *et al* 2007; Mosavat *et al* 2011).

The corrosion resistance and mechanical properties of ZnNi alloy coating was significantly influenced by the morphology, microstructure and composition of the deposit. These in turn depend on bath composition, additives, current density, temperature and thickness of electrodepostion (Ravindran and Muralidharan 2007; Rizwan *et al* 2007; Shivakumara *et al* 2007; Rahman *et al* 2009). Chitharanjan Hegde *et al* (2010) reported the increase of nickel content, corrosion resistance and Vickers microhardness of the deposit with applied current density up to 3 A dm^{-2}. Eliaz *et al* (2010) studied that ZnNi coating showed higher thickness, nickel content, hardness and corrosion resistance with increase in current density up to 4 A dm^{-2}. Hammami *et al* (2013) studied the effect of diethanolamine (DEA) and triethanolamine (TEA) on ZnNi alloy coating from an acid bath. The ZnNi coating obtained was fine grain, corrosion resistant and contains Zn and γ-phases. Rahman *et al* (2009) had found the refinement of crystal size, increase in nickel content, corrosion resistance and microhardness of ZnNi alloy coatings with applied current density in sulphate bath. Albalat *et al* (1990) established the formation of smooth and bright ZnNi deposit with good corrosion resistance in presence of phenolic derivative from chloride bath at lower nickel percentage. De Oliveira and Carlos (2009) reported the formation of ZnNi deposit with coalesced globular crystallites of small size in presence of mannitol.

*Author for correspondence (drtvvenkatesha@yahoo.co.uk)

Although additives, deposition current density and thickness play important role in improving properties of ZnNi alloy deposit, very little focus was given.

The purpose of the present investigation is to obtain smooth, uniform and bright ZnNi electrodeposit from acid sulphate bath using additive EV. Correspondingly, we have made a systematic study of effect of EV on current efficiency, throwing power, deposition–dissolution behaviour, surface morphology, microstructure, microhardness and corrosion resistance of ZnNi alloy deposit. At the same time, influence of current density and coating thickness on corrosion resistance of bright ZnNi deposit was studied.

2. Experimental

ZnNi alloy plating baths were prepared using analytical grade, SD–Fine chemicals (Mumbai, India) and Millipore (Elix France) water. 2·7 pH of bath solution was adjusted by using 10% H_2SO_4 and $NaHCO_3$ solutions. 4×4 cm^2 mild steel plates were mechanically polished, degreased with vapours of trichloroethylene and subjected to water wash. The anode was 99·9% zinc and its surface was activated each time by dipping in 10% HCl for few seconds and washed with water. Equal area of an anode and a cathode was maintained throughout the deposition process. Deposited plates were given bright dip in 1% HNO_3 for 2 s, followed by water wash and drying.

Current efficiency (CE) was calculated based on Faraday law, using mass gained, charge passed and chemical composition of the deposit.

$$\mathrm{CE} = \frac{wF}{It} \sum \frac{c_i n_i}{M_i} \times 100, \quad (1)$$

where w is the measured mass of the alloy deposit (g), I the total current passed (Å) in time interval, t (s), c_i the weight fraction of the alloy element in deposit, n_i the number of electrons transferred per atom of each metal, M_i the atomic mass of that element (g mol^{-1}) and F the Faraday's constant (96,500 C mol^{-1}). While the thickness of the coating was estimated by Faraday's law and comparing with measurements made using digital thickness meter.

The throwing power of the bath was measured using Haring–Blum cell.

$$\text{Throwing power } \% = \frac{L - M}{L + M - 2} \times 100, \quad (2)$$

where L is the ratio of distance from the anode of farther and nearer cathodes, respectively, and M the ratio of deposit weights obtained on nearer and farther cathodes.

Chemical composition of ZnNi alloy coating was estimated by colorimetric method. The known weight of deposit was dissolved in 5% HCl. The nickel(II) was precipitate, using dimethylglyoxime to get red coloured chelate compound formed quantitatively in a solution. The chelated compound was dissolved in alcohol and finally estimated calorimetrically (Jeffery *et al* 1989).

Cyclic voltammetric studies were carried out in a conventional three-electrode cell in order to understand the process of ZnNi alloy electrodeposition and to identify the effect of EV. Glassy carbon disc of surface area, 0·07065 cm^2 was employed as working electrode. The saturated calomel electrode (SCE) and platinum wire were employed as reference and counter electrodes, respectively. The surface of glassy carbon electrode was prepared by polishing with 0·05 μm alumina, agitated ultrasonically for 15 min in 10% HCl and then, washed with running water. For all electrochemical measurements, CHI660C electrochemical analyser (USA) was used.

FT–IR spectrum was analysed using instrument GX spectrometer, Perkin Elmer, USA. The sample and detector chambers were purged with nitrogen gas before starting the experiments.

Surface morphology of the deposits was analysed by scanning electron microscope (FESEM, LE01530-VP) images. Also grain size and preferred crystal orientations of the deposits were examined by X-ray diffraction (XRD) studies using PANalytical X'pert Pro powder diffractometer. Average grain size of deposit was calculated using Debye Scherer's equation

$$D = k\lambda/\beta \cos\theta,$$

where $k = 0{\cdot}9$, β is full width at half maximum, θ the reflectance angle and $\lambda = 1{\cdot}546$ Å wave length of radiation used (Cullity *et al* 1978).

The preferred orientations of the deposits were determined by using Muresan's method by calculating the texture coefficient (T_c) using the equation

$$T_c = \frac{I(hkl)}{\sum I(hkl)} \frac{\sum I_0(hkl)}{I_0(hkl)} \times 100, \quad (3)$$

where $I(hkl)$ is the peak intensity of ZnNi electrodeposits and $\sum I$ the sum of intensities of independent peaks. The index 0 refers to the intensities for the standard zinc sample (JCPDS card number: 00-004-0831) (Mouanga *et al* 2007).

Knoop microhardness of the deposits was determined by indentation technique with a weight of 25 and 50 g for 5 s using Clemex microhardness tester, made in Japan. Four spots at different locations on each coating surface were used for measurement. The average value was reported as microhardness.

The reflectance values of zinc deposit were recorded using NOVO gloss meter, referenced against a vacuum-coated silver mirror. The reflectivity of silver mirror was set at 100% at an angle of 60°. The measurements were carried out at different points on the coating surface and the average values have been reported.

Table 1. Optimized bath composition and operating conditions.

Bath constituents	Concentration (g L^{-1})	Operating conditions
$ZnSO_4 \cdot 7H_2O$	250	Anode: zinc plate (99·9%)
$NiSO_4 \cdot 6H_2O$	20	Cathode: mild steel plate
Na_2SO_4	40	pH: 2·7, temperature: 298 K
H_3BO_3	8	Plating time: 10
CTAB	2	Cell current: 1A
Ethyl vanillin	0·24	Current density: 0·2–5·6 A dm^{-2}

The corrosion behaviour of the coating was studied by potentiodynamic polarization and electrochemical impedance spectroscopy (EIS) technique in 3·5% NaCl solution. The standard three-electrode cell was used. The ZnNi coating with 1 cm^2 exposed surface area was employed as working electrode. The potential was measured with respect to SCE, while the Pt wire was used as counter electrode. The polarization curves were recorded at a sweep rate of 0·1 mV s^{-1} in the potential range + 0·2 to − 0·2 V between open circuit potentials. Corrosion parameters such as corrosion potential (E_{corr}), corrosion current (I_{corr}), anodic (ba)/cathodic (bc) tafel slopes and corrosion rate were obtained from the software installed in the instrument. The electrochemical impedance measurements were carried at open circuit potential (OCP) in the frequency range of 1 mHz–10 kHz with 5 mV sine wave as excitation signal. Impedance data were analysed using Zsimp-Win 3.21 software.

3. Results and discussion

The bath constituent and operating conditions were optimized by Hull cell experiments to get bright deposit over wide range of current density. During Hull cell experiments, concentration of one constituent was varied in constant increments, while keeping other constituents at their selected concentrations. The particular concentration at which bright, uniform deposit was produced over wide range of current density was fixed as optimum concentration. The procedure was repeated for all bath constituents and operating conditions. The optimum bath composition and operation conditions for bright ZnNi alloy electrodeposition selected for further studies are given in table 1.

Bath solution in table 1 gave dull deposit with 7% reflectance in absence of EV. While in presence of EV, mirror bright deposit with 78% reflectance was obtained. The brightening agent EV in bath solution (table 1) produced bright deposit in the current density ranged from 0·2 to 5·6 A dm^{-2}. The brightening agent play major role on improving efficiency, hardness and corrosion resistance of coating. Hence, in order to know the influence EV, a detailed study was undertaken in presence and absence of brightening agent in optimized bath (table 1). The current density and thickness of deposition directly control the iron content of coating. Hence, considerably affect on corrosion resistance of bright electrodeposit. Thus, corrosion resistance of bright ZnNi deposit was analysed at different deposition current density and thickness.

3.1 *Current efficiency, throwing power and chemical composition*

At 4 A dm^{-2} current efficiency and throwing power, respectively, in absence of EV were found to be 58 and 16%, whereas these enhance to 86 and 33% in presence of EV. Thus, presence of EV improves current efficiency and throwing power of optimized bath solution during electrodeposition.

Current efficiency and throwing power of optimized bath solution were measured at different current densities from 1 to 5 A dm^{-2} (table 2). At lower current density (1 A dm^{-2}), the current efficiency was found to be 74%. The maximum efficiency of 86% was observed at 4 A dm^{-2}. Further increase in current density, reduces efficiency to 84% at 5 A dm^{-2}.

Throwing power of optimized bath at lower current density (1 A dm^{-2}) was found to be 16%. Throwing power was enhanced to 33% at 4 A dm^{-2}. Further increase in current density above 4 A dm^{-2}, decreases throwing power to 31% at 5 A dm^{-2}.

Chemical composition of ZnNi alloy deposit was analysed in absence and presence of EV at 4 A dm^{-2}. The nickel content of deposit in absence of EV was found to be 4·3%, however, reduces to 1·9% in presence of EV.

ZnNi deposits were obtained at different current densities (1–6 A dm^{-2}) and thicknesses (3–22 μm) on copper plates and composition of alloy was estimated. The composition of analysed ZnNi alloy showed that nickel percentage in deposit decreases with increase in deposition current density and thickness. Figure 1(a and b) shows the effect of current density (cd) and thickness on nickel content of ZnNi alloy coating.

3.2 *Cyclic voltammetric studies*

Effect of EV on electrochemical behaviour of ZnNi alloy was analyzed by cyclic voltammetric studies. 0·34 M

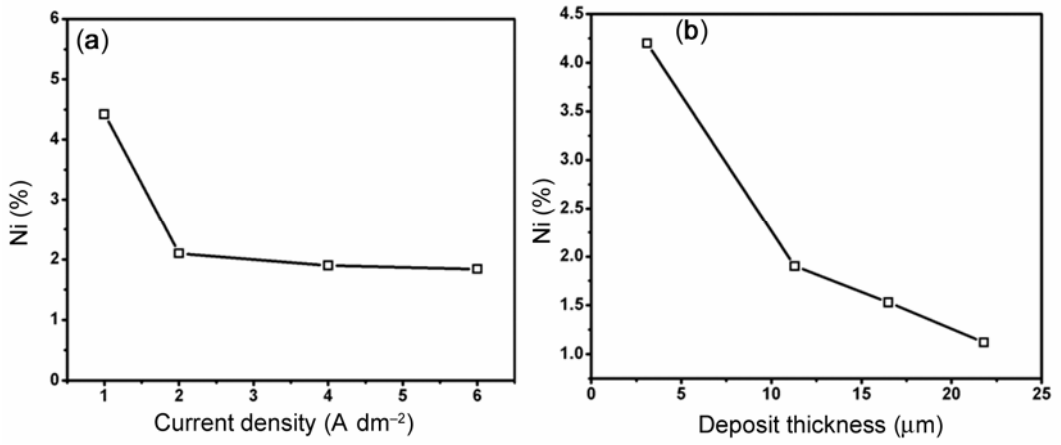

Figure 1. Effect of (**a**) current density and (**b**) thickness of coating on the composition of ZnNi deposit obtained from optimized bath.

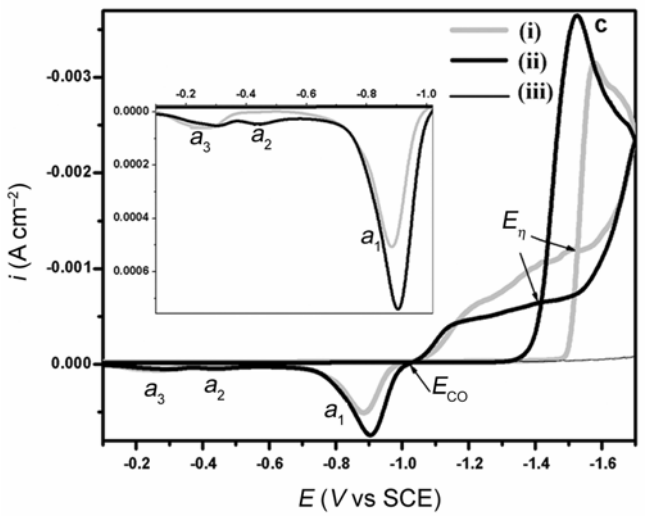

Figure 2. Cyclic voltammograms obtained from bath 0·34 M $ZnSO_4{\cdot}7H_2O$, 0·076 M $NiSO_4{\cdot}7H_2O$, 0·065 M H_3BO_3 and 2 M Na_2SO_4 in (i) absence and (ii) presence of 1·5 mM EV and (iii) in supporting electrolyte 2 M Na_2SO_4, 0·065 M H_3BO_3 and 1·5 mM EV.

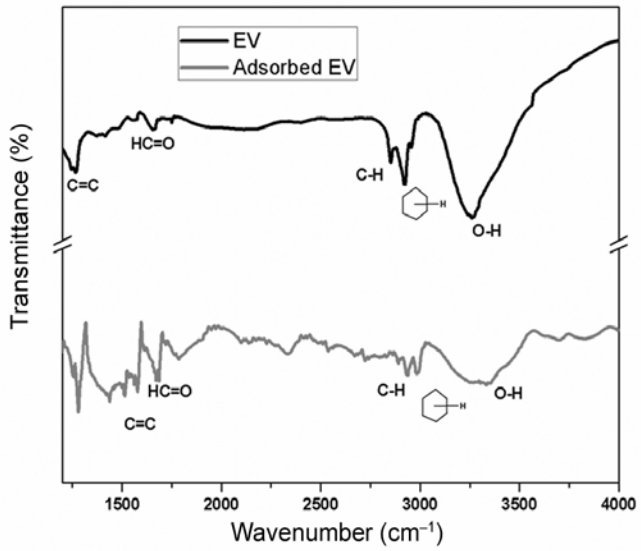

Figure 3. FT–IR spectra of EV powder sample and adsorbed EV on steel.

Table 2. Current efficiency and throwing power of optimum bath at different current densities.

Current density (A dm^{-2})	Current efficiency (%)	Throwing power (%)
1	74	16
2	77	26
3	81	28
4	86	33
5	84	31
6	81	30

$ZnSO_4{\cdot}7H_2O$, 0·076 M $NiSO_4{\cdot}7H_2O$, 2 M Na_2SO_4 and 0·065 M H_3BO_3 solutions was used (figure 2). The potential scan was started in the cathodic direction from the rest potential at scan rate 50 V s^{-1}.

The preliminary experiments showed that EV has no electrochemical activity under the experimental condition studied (figure 2(iii)). In absence of EV (figure 2(i)) during cathodic scan, the deposition peak potential was –1·53 V (peak c). This peak was associated with simultaneous reduction of both Zn^{2+} to Zn and Ni^{2+} to Ni. On reversing the sweep direction, two current crossovers appear in the cathodic region. The potential at which the crossover occurs at more cathodic region was known as nucleation overpotential (E_η) (Albalat *et al* 1990). And the second crossover at zero current region (–1·019 V) was known as the crossover potential (E_{co}) (Fletcher *et al* 1983). The two crossovers were characteristics of three-dimensional (3D) nucleation and subsequent crystal growth process (Gunawardena *et al* 1982). In the absence

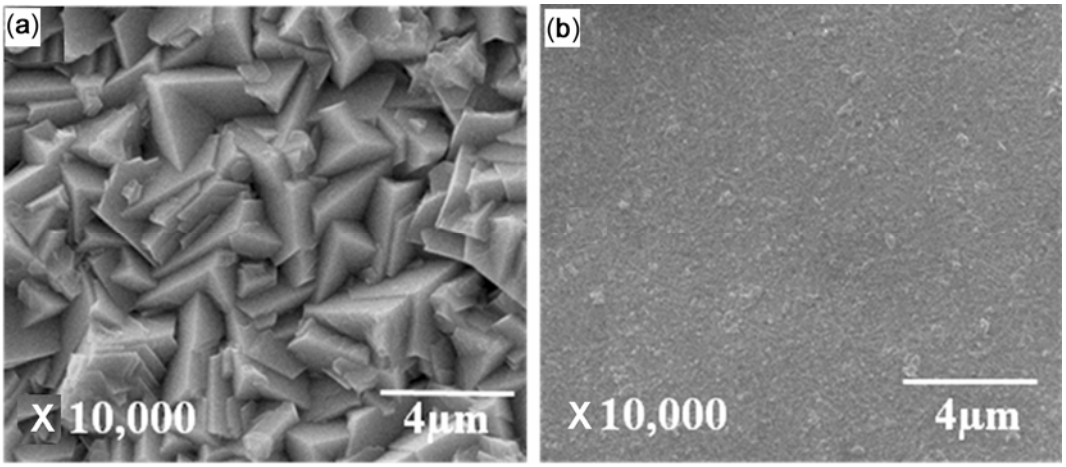

Figure 4. SEM images of (**a**) dull and (**b**) bright ZnNi electrodeposit obtained in absence and presence of EV at 4 A dm^{-2}.

of EV, three oxidation peaks (a_1, a_2 and a_3) are observed in the potential range −1 to −0·1 V vs SCE. The multiple peaks detected during the electrochemical oxidation of alloys are due to dissolution of metals in the alloy via different intermediate phases (Jovic *et al* 1988). The three anodic dissolution peaks for ZnNi alloy, corresponding to the dissolution of three phases in deposit η-phase, δ-phase (Ni_3Zn_{22}) and γ-phase (Ni_5Zn_{21}) (Abou-Krisha 2005; Abou-Krisha *et al* 2008). The first anodic peak (a_1) at a potential of –0·905 V corresponds to the oxidation of zinc from the η-phase (zinc-rich phases), which was almost pure zinc phase. The second (a_2) and third (a_3) anodic peaks at potential –0·444 and –0·314 V, respectively, corresponding to the dissolution of zinc from δ- and γ-phases (or nickel-rich phases). Thus, the voltammetric response gives information regarding the characteristics of components of the alloy and structure of the deposited phases.

In presence of EV, the plating bath deposition potential was shifted to –1·58 V, more negative potential and deposition current density also decreases compared to absence of EV. These results indicate that the EV acts at the interface, creating barrier at the vicinity of the electrode and hinders the discharge of metal ions lead to the reduction of grain size of the deposit (Oniciu and Muresan 1991; Ballesteros *et al* 2007). In presence of EV, two oxidation peaks a_1 and a_3 were observed at − 0·882 and –0·273 V. The first anodic peak, a_1 corresponds to the oxidation of zinc from the η-phase (zinc-rich phase) and whereas broad second anodic peak, a_3 corresponds to dissolution of zinc or nickel from γ- and δ-phases (or nickel-rich phases). The oxidation peaks are slightly shifted to more positive potential. This indicated that oxidation of ZnNi alloy become more difficult in presence of EV and thus, deposit obtained was more uniform and compact.

3.3 *FT–IR analysis*

FT–IR spectra of EV powder showed peaks at 3334 cm^{-1} (O–H stretch), 2993·6 cm^{-1} (ring hydrogen stretching), 2935·2 cm^{-1} (C−H stretching in ethoxy [O–C_2H_5] groups), 1685·7 cm^{-1} (C=O stretching of aldehyde group), 1400–1600 cm^{-1} (ring C=C stretching). Prior to FT–IR analysis, polished steel sample was placed in 0·24 g L^{-1} EV solution for 1 h and dried. The stretching peaks corresponding to ring hydrogen, ring C=C, ethoxy C–H and aldehydic C=O were shifted to lower wavenumber. The lower wavenumber means increase in wavelength (red shift) was noticed. This indicated the adsorption of EV on steel surface through interaction of aldehydic C=O, ethoxy oxygen and aromatic ring with plating surface.

3.4 *Surface morphology and phase composition of deposit*

Figure 4 shows SEM images of the dull and bright deposit obtained in absence and presence of EV, respectively. The dull deposit (without EV) showed coarse-grained deposit having randomly distributed nano-laminated thin hexagonal platelets. Whereas, bright deposit showed fine grain, uniform, smooth and compact deposit without any pin holes or pores. This indicated that EV promotes the refinement of grain size by enhancing the number of nucleation sites and retarding the growth of nuclei during deposition.

XRD pattern of dull and bright ZnNi alloy deposit are shown in figure 5. All the deposits were crystalline in nature and have hexagonal structure. The dull ZnNi alloy electrodeposit exhibits three main phases: η-phase, δ-phase and γ-phase. An η-phase contains very high amount of zinc which was solid solution of nickel in zinc. While the δ- and γ-phases were intermediate phases with

composition of Ni_3Zn_{22} and Ni_5Zn_{21}, respectively (Abou-Krisha 2005; Abou-Krisha *et al* 2008). Whereas, bright ZnNi alloy coating contain more predominantly η-phase. The relative intensities of the phases in both the coatings change with deposited layers thickness which has different compositions. Also, with increase in zinc content of the deposit, the η-phase becomes more intense. The average grain size of dull and bright deposits were found to be 87 and 35 nm, respectively. Thus, refinement of grain size of the deposit was noticed.

To know the preferred orientation of ZnNi alloy deposit, texture coefficient was calculated for each peak in diffraction patterns (figure 5). The corresponding T_c values are presented as bar diagram in figure 6. In dull deposit, T_c value was maximum for (102) plane. Hence, (102) was the preferred orientation of the dull deposit. While in case of bright deposit, (110) was the preferred orientation with maximum T_c value of 52%. The preferential adsorption EV on different crystallographic planes changes the preferred orientation of deposit from (102) to (110).

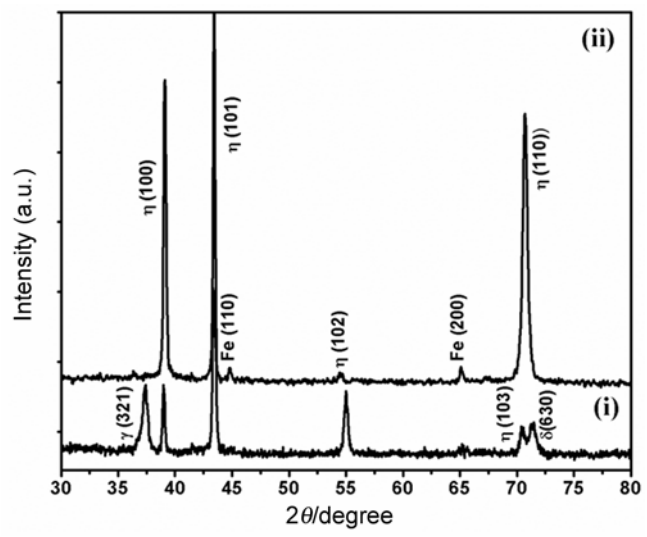

Figure 5. X-ray diffraction patterns of (**i**) dull and (**ii**) bright ZnNi electrodeposit obtained in absence and presence of EV at 4 A dm^{-2}.

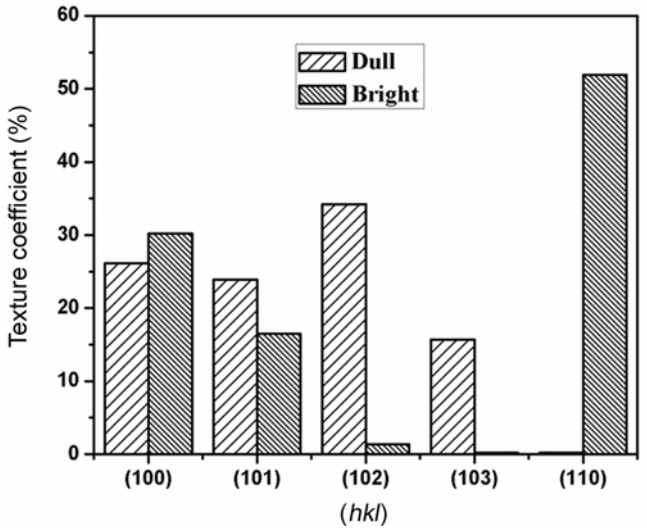

Figure 6. Percent T_c values as a function of crystallographic plane for dull and bright ZnNi deposit obtained in absence and presence of EV at 4 A dm^{-2}.

3.5 *Hardness of deposit*

Figure 7 shows Knoop microhardness of dull and bright ZnNi deposits at 4 A dm^{-2} with test load of 25 gf. The hardness of dull and bright ZnNi alloy deposits were found to be 98 and 120 H_K, respectively. According to earlier literature, deposit containing prismatic preferred orientation (110) exhibit higher hardness. Hence, presence of (110) preferred orientation was responsible for the higher hardness of bright deposit (Saber *et al* 2003).

3.6 *Adherence ductility and porosity of the deposit*

To test the adhesion and ductility of bright ZnNi deposit, steel plates of 10 × 2 cm^2 area were plated. The samples were subjected to bending test through 180°. No crack or peel off the deposit was noticed even after 180° bending through many cycles. This confirms the good adherence and ductility of deposit to base metal.

Porosity tests were conducted on bright ZnNi alloy-coated steel panels (6 × 4 cm^2). A filter paper soaked in potassium ferricyanide solution (1%) was placed on alloy-coated steel panels. There was no blue spot at sufficient thickness indicating pore-free nature of alloy deposits.

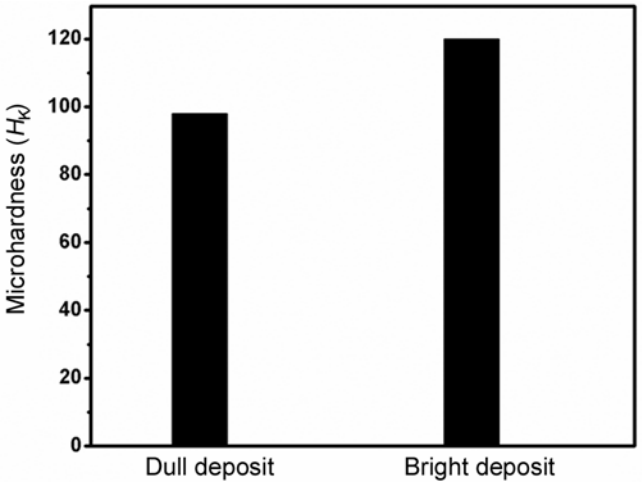

Figure 7. Microhardness of dull and bright ZnNi deposit obtained in absence and presence of EV at 4 A dm^{-2}.

Table 3. Corrosion parameters from tafel plots at different thicknesses and current densities.

Coating		E_{corr} (V/SCE)	I_{corr} (A cm^{-2})	β_c (mV dec^{-1})	β_a (mV dec^{-1})	Corrosion rate (g/h)
Dull at 4 A dm^{-2}		−1·088	27·28	5·457	13·031	$3{\cdot}32 \times 10^{-5}$
Bright coating at different thicknesses (μm)	3·1	−1·036	$4{\cdot}876 \times 10^{-6}$	5·487	18·542	$5{\cdot}947 \times 10^{-6}$
	11·3	−1·068	$9{\cdot}546 \times 10^{-6}$	8·089	15·269	$1{\cdot}164 \times 10^{-5}$
	16·5	−1·074	$4{\cdot}746 \times 10^{-5}$	7·147	14·212	$5{\cdot}79 \times 10^{-5}$
	21·8	−1·101	$1{\cdot}395 \times 10^{-4}$	6·948	11·365	$1{\cdot}704 \times 10^{-4}$
Bright coating at different current densities (A dm^{-2})	2	−1·048	$5{\cdot}261 \times 10^{-6}$	2·825	23·92	$7{\cdot}213 \times 10^{-6}$
	4	−1·068	$9{\cdot}546 \times 10^{-6}$	8·089	15·269	$1{\cdot}164 \times 10^{-5}$
	6	−1·072	$4{\cdot}859 \times 10^{-5}$	7·42	13·45	$5{\cdot}927 \times 10^{-5}$

Table 4. Impedance data of bright ZnNi alloy coating obtained at different thicknesses and current densities.

ZnNi coating		R_S ($\mu\Omega$ cm^2)	C_1 (μF cm^{-2})	R_1 (Ω cm^2)	C_2 (μF cm^{-2})	R_2 (Ω cm^2)	C_3 (mF cm^{-2})	R_3 (Ω cm^2)	R_P (Ω cm^{-2})
Dull at 4 A dm^{-2}		9·66	0·285	70·4	6·335	506·5	0·877	635·2	1212·1
Bright coating at different thicknesses (μm)	3·1	46·01	0·269	79·84	4·661	1465	0·132	1055	2599·84
	11·3	53·82	0·248	79·21	5·358	612·5	0·155	674·5	1366·21
	16·5	12·22	0·354	110·1	9·04	533·6	0·203	496·5	1140·2
	21·8	5·631	0·745	80·54	7·449	213	0·922	197·3	490·84
Bright coating at different current densities (A dm^{-2})	2	10·71	0·373	91·05	2·036	461·4	0·136	930·4	1482·85
	4	53·82	0·248	79·21	5·358	612·5	0·155	674·5	1366·21
	6	15·67	0·460	81·07	8·635	606·9	0·221	600·6	1288·57

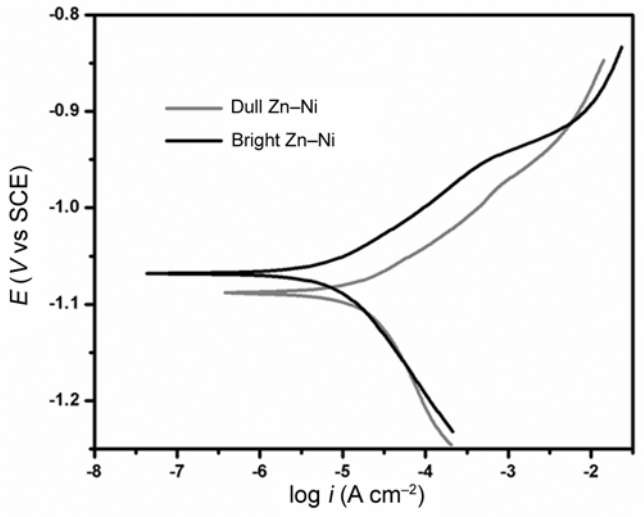

Figure 8. Potentiodynamic polarization curves for dull and bright ZnNi deposit obtained in absence and presence of EV at 4 A dm^{-2}.

3.7 *Corrosion studies*

Form earlier reports, it was clear that ZnNi alloys coating were found to exhibit excellent corrosion resistance than other zinc alloys. Further additives, EV introduced in the electroplating bath develop smooth bright fine grain deposit and have a beneficial effect on improving corrosion resistance of ZnNi alloy coating. Also, protection ability of alloy coating varies with deposition current density and thickness at the same current density due to difference in chemical composition of coating. Hence, it is required to study the effect of EV, current density and thickness on the protection ability of deposit generated from optimized bath.

3.7a *Potentiodynamic polarization studies*: Figure 8 shows tafel curves recorded for dull and bright ZnNi alloy coatings obtained in absence and presence of EV at 4 A dm^{-2}, respectively. The corrosion parameters obtained from tafel curves are tabulated in table 3. E_{corr} value shifted to more noble direction, I_{corr} reduced and smaller corrosion rate was noticed in bright deposit compared to dull deposit. Anodic behaviour of bright Zn–Ni coatings are more polarized than dull coating. So metal dissolution takes place at higher potential than dull coating and it indicated more corrosion resistance property of bright coating. Metal dissolution was hindered and decomposition potential of the metal reached at –2 V and it is greater than dull deposition and there was not much difference observed in cathodic behaviour. Thus, bright ZnNi coating exhibits higher corrosion resistance.

The good protection ability of bright ZnNi alloy coating depends on texture, morphology and chemical composition. In the fine grained bright deposit, higher binding energy of atom and rapid formation of oxide protection layer hinders the oxidation of atoms. The codeposition of nickel with zinc in the coating enhances the corrosion

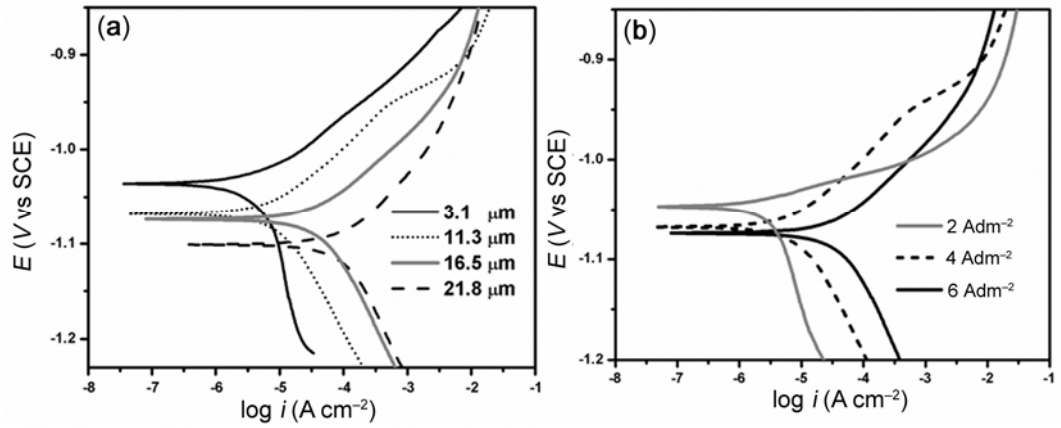

Figure 9. The potentiodynamic polarization curves for bright ZnNi coating obtained in presence of EV at different (**a**) thicknesses and (**b**) current densities.

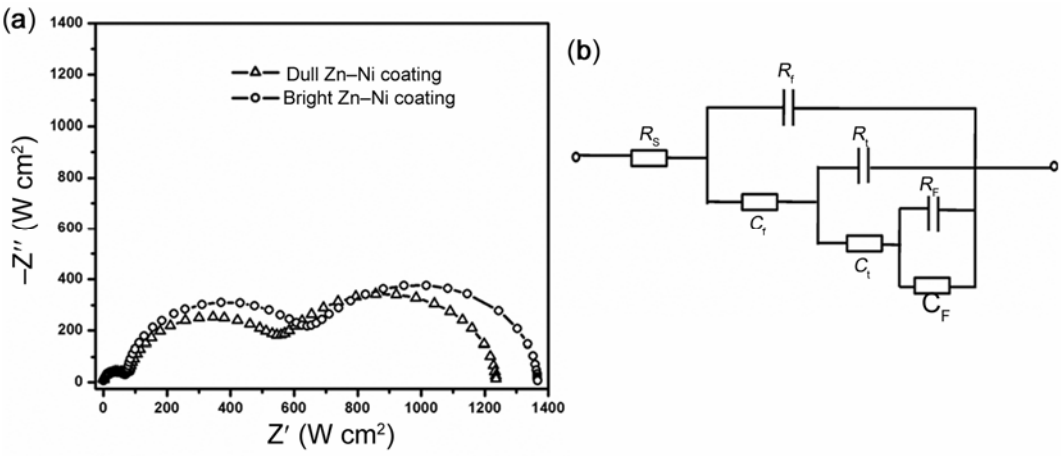

Figure 10. Niquist plots of (**a**) dull and bright ZnNi alloy deposits at 4 A dm^{-2} obtained in absence and presence of EV at 4 A dm^{-2} and (**b**) its equivalent electrical circuit.

resistance of deposit. Also, microstructure of bright zinc deposit contains only η-phase (presence of single phase in coating result in smaller corrosion). Thus, bright deposit showed good corrosion protection.

Figure 9 shows tafel curves recorded for coating obtained at different thicknesses and current densities. The corrosion parameters obtained from tafel curves are listed in table 3. In figure 9(a), polarization effect was increased with increase in thickness of the coating and it was more polarized and maximum at 21·8 μm and minimum corrosion rate was observed. The corrosion rate of the deposit increase from 5·947 μg h^{-1} to 0·17 mg h^{-1} with increase in thickness of the deposit from 3 to 23 μm. Due to hydrogen evolution during deposition, zinc hydroxide layer was formed. This hydroxide strongly suppresses further reduction of nickel (more noble metal). Thus, nickel was hardly co-deposited with zinc. Hence, percentage of nickel decreases with increase in thickness of the deposit. This in turn leads to higher I_{corr}, shift of E_{corr} to more negative direction and increase of corrosion in thicker ZnNi coating. The bright ZnNi alloy coating obtained at different current densities of 2, 4 and 6 A dm^{-2} was more resistant than dull deposit. In figure 9(b), more polarization was observed with increase in current density in cathodic direction. Controversial behaviour was observed in anodic direction, at 2 A dm^{-2} more polarized and dissolution of metal taking place at higher potential and gives more corrosion resistance property. But, I_{corr} increases and E_{corr} shifts to less noble direction for deposit obtained at higher current density and this indicated lowering of corrosion resistance of the deposit.

3.7b *Electrochemical impedance studies*: Figure 10(a) shows the Nyquist plots of dull and bright ZnNi alloy deposit. The plots displayed three capacitive loops. Impedance values of bright deposits are higher than

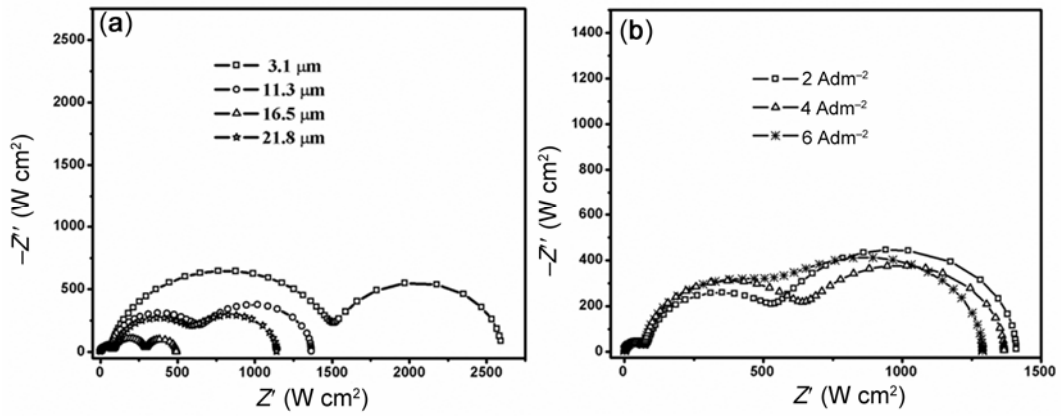

Figure 11. Niquist plots of bright ZnNi alloy coating obtained in presence of EV at different (**a**) thicknesses and (**b**) current densities.

dull deposit. The equivalent circuit proposed to analyse impedance spectra is shown in figure 10(b) and data are listed in table 5. The polarization resistance (R_P) values were calculated by adding R_1, R_2 and R_3 resistance values (table 4). The R_P increased and double layer capacitance decreased in bright deposit compared to dull deposit. The higher R_P value was due to both charge transfer resistance and increase in the thickness of the corrosion product layer. The decrease in double layer capacitance resulted from a reduction in the local dielectric constant and/or from increased double layer thickness (Vlasa *et al* 2010).

The impedance plot of bright ZnNi deposit obtained at different thicknesses and current densities are shown in figure 11. The corresponding impedance data are given in table 4. The R_P decreased and double layer capacitance increased with increase in coating thicknesses and current densities. Thus, deposit obtained at higher current density and thickness showed lower corrosion resistance.

4. Conclusions

The brightener, EV, gave smooth, uniform, fine-grained and bright ZnNi alloy coating in the current density range of 0·2–5·6 A dm^{-2}. The EV improves bath properties like throwing power and current efficiency to 33 and 86%, respectively. Bright coating exhibits good deposit properties like adherence, ductility, microhardness and corrosion resistance compared to dull deposit. Also, corrosion rate of bright ZnNi coating was lower at higher current density and thickness.

Acknowledgements

Authors gratefully acknowledge the Kuvempu University, Shimoga, India for providing the lab facilities to bring about this work.

References

Abou-Krisha M M 2005 *Appl. Surf. Sci.* **252** 1035
Abou-Krisha M M, Rageh H M and Matter E A 2008 *Surf. Coat. Technol.* **202** 3739
Albalat R, Gomez E, Muller C, Sarret M and Valli E 1990 *J. Appl. Electrochem.* **20** 635
Bajat J B, Petrovic A B and Maksimovic M D 2005 *J. Serb. Chem. Soc.* **70** 1427
Ballesteros J C, Diaz-Arista P, Meas Y, Ortega R and Trejo G 2007 *Electrochim. Acta* **52** 3686
Brooks I and Erb U 2001 *Scr. Mater.* **44** 853
Cullity B D 1978 *Elements of X-ray diffraction* (Philippines: Wesley Publishing Company, Inc.) 2nd edn
Chitharanjan Hegde A, Venkatakrishna K and Eliaz N 2010 *Surf. Coat. Technol.* **205** 2031
De Oliveira E M and Carlos I A 2009 *J. Appl. Electrochem.* **39** 1849
Eliaz N, Venkatakrishna K and Chitharanjan Hegde A 2010 *Surf. Coat. Technol.* **205** 1969
Fletcher S, Halliday C S, Gates D, Westcott M, Lwin T and Nelson G 1983 *J. Electroanal. Chem.* **159** 267
Gunawardena G, Hills G and Montenegro I 1982 *J. Electroanal. Chem.* **138** 241
Hammami O, Dhouibi L, Bercot P, Rezrazi E M and Triki E 2013 *Can. J. Chem. Eng.* **91** 19
Jeffery G H, Bassett J, Mendham J and Denney R C 1989 *Vogel's text book of quantitavtive chemical analysis* (New York: John Wiley & Sons, Inc.) 5th edn, p. 693
Jovic V D, Zejnilovic R M, Despic A R and Stevanoic J S 1988 *J. Appl. Electrochem.* **18** 511
Kautek W, Sahre M and Paatsch W 1994 *Electrochim. Acta* **39** 1151
Li M, Luo S, Qian Y, Zhang W, Jiang L and Shen J 2007 *J. Electrochem. Soc.* **154** D567
Kim H, Popov B A and Chen K S 2003 *J. Electrochem. Soc.* **150** C81
Mosavat S H, Bahrololoom M E and Shariat M H 2011 *Appl. Surf. Sci.* **257** 8311
Mouanga M, Ricq L, Douglade J and Bercot P 2007 *J. Appl. Electrochem.* **37** 283

Oniciu L and Muresan L 1991 *J. Appl. Electrochem.* **21** 565
Pech-Canul M A, Ramanauska R and Maldonado L 1997 *Electrochim. Acta* **42** 255
Pushpavanam M 2000 *Bull. Electrochem.* **16** 559
Pushpavanam M, Natarajan S R, Balakrishnan K and Sharma L R 1991 *J. Appl. Electrochem.* **21** 642
Rizwan R, Mehmood M, Imran M, Ahmad J, Aslam M and Javed I A 2007 *Mater. Trans.* **48** 1558
Ravindran V and Muralidharan V S 2007 *Portugaliae Electrochim. Acta* **25** 391
Rahman M J, Sen S R and Moniruzzaman M 2009 *J. Mech. Eng.* **40** 9
Sachin H P, Ganesha Achary, Arthoba Naik Y and Venkatesha T V 2007 *Bull. Mater. Sci.* **30** 57
Saber K K, Fedkiw C C and Fedkiw P S 2003 *Mater. Sci. Eng.* **A341** 174
Shivakumara S, Manohar U, Arthoba Naik Y and Venkatesha T V 2007 *Bull. Mater. Sci.* **30** 455
Vlasa A, Varvara S, Pop A, Bulea C and Muresan L M 2010 *J. Appl. Electrochem.* **40** 1519